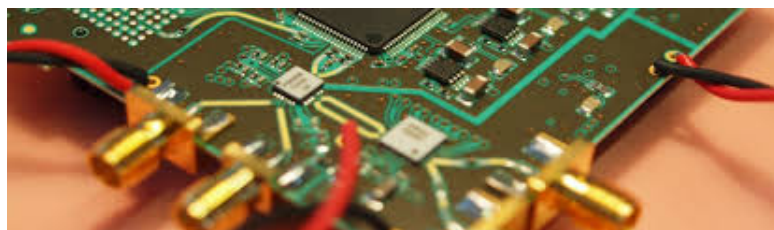


# A Terabit sampling system with a photonics time-stretch ADC

Master Thesis  
of

Olena Manzhura

at the Institute for Data Processing and Electronics (IPE)



Reviewer: Prof. Dr. Anke-Susanne Müller (LAS)  
Second Reviewer: Dr. Michele Caselle (IPE)

15.11.2020 – 13.08.2021



# Declaration

I hereby declare that I wrote my master thesis on my own and that I have followed the regulations relating to good scientific practice of the Karlsruhe Institute of Technology (KIT) in its latest form. I did not use any unacknowledged sources or means, and I marked all references I used literally or by content.

Karlsruhe, 13.08.2021, \_\_\_\_\_  
Olena Manzhura

Approved as an exam copy by

Karlsruhe, 13.08.2021, \_\_\_\_\_  
Prof. Dr. Anke-Susanne Müller (LAS)



# **Abstract**



# Zusammenfassung



# Résumé



# Contents

<b>1. Introduction</b>	<b>1</b>
<b>2. Theoretical Fundamentals</b>	<b>3</b>
2.1. Coherent Synchrotron Radiation . . . . .	3
2.1.1. Micro-Bunching Instabilities . . . . .	4
2.2. Electro-Optic Techniques and Time-Stretch . . . . .	6
2.2.1. Scanning-Type Electro-Optic Sampling . . . . .	6
2.2.2. Spectrally Resolved Electro-Optic Detection . . . . .	6
2.2.3. Photonic Time-Stretch Technique . . . . .	7
2.2.4. Time-Stretched Spectrally-Encoded Electro-Optic detection . . . . .	7
2.3. Analog-To-Digital Converters . . . . .	8
2.3.1. Sampling Theory . . . . .	8
2.3.2. Characteristics of Analog-To-Digital-Converters . . . . .	9
2.3.2.1. Quantization Noise . . . . .	10
2.3.2.2. Static parameters . . . . .	11
2.3.2.3. Dynamic performance . . . . .	12
2.3.3. Interleaving . . . . .	13
2.4. RF/Microwave Design Basics . . . . .	14
2.4.1. General Techniques/Strategies? . . . . .	14
2.4.2. Coplanar Waveguides . . . . .	14
<b>3. Design and Development of the System</b>	<b>17</b>
3.1. General architecture . . . . .	17
3.1.1. KAPTURE-2 . . . . .	17
3.1.2. New System THERESA . . . . .	19
3.1.3. Requirements . . . . .	20
3.2. Design of the front-end card . . . . .	22
3.2.1. Sampling-Channel . . . . .	22
3.2.2. Clocking . . . . .	22
3.2.3. Power Supply . . . . .	23
3.3. PCB-Layout . . . . .	24
3.3.1. Floor Planning . . . . .	24
3.3.2. Transmission lines . . . . .	24
3.4. Firmware . . . . .	25
3.4.1. General Design . . . . .	25
3.4.1.1. Firmware for Front-End Card . . . . .	25
3.4.1.2. Data Capture . . . . .	25
3.4.1.3. Visualization . . . . .	25
<b>4. Characterization</b>	<b>27</b>
4.1. Evaluation of the ZCU216 Board/ADCs . . . . .	27
4.1.1. Measurements with Xilinx XM655 add-on card . . . . .	27

<b>5. Conclusions and Outlook</b>	<b>29</b>
5.1. Measurements with the developed front-end card . . . . .	29
<b>Acknowledgements</b>	<b>29</b>
<b>Appendix</b>	<b>33</b>
A. QuickStart Guide for Evaluation of ZCU216 Board . . . . .	33
B. 3D model of front-end card . . . . .	33
C. Code . . . . .	33
<b>Bibliography</b>	<b>37</b>

# List of Figures

2.1.	Basic scheme of an electron storage ring (redrawn from [Rou14]) . . . . .	3
2.2.	Electromagnetic spectrum . . . . .	4
2.3.	Placeholder [Rot18] . . . . .	4
2.4.	Electrons interact with their own radiation [BBB <sup>+</sup> 19] . . . . .	5
2.5.	Facility [Rot18] . . . . .	5
2.6.	Scheme of Scanning-Type Electro-Optical Sampling System [Rou14] . . . . .	6
2.7.	Scheme of Spectrally Encoded Electro-Optical Detection System [Rou14] . . . . .	6
2.8.	Electro-Optical Time-Stretch Technique [SELP <sup>+</sup> 16] . . . . .	7
2.9.	Analog signal with frequency $f_a$ sampled at $f_s$ respecting (A) and not respecting (B) the Nyquist criteria. Figure 2.9b shows the effect of case B in time domain. [Kes05] . . . . .	8
2.10.	Track-And-Hold-Amplifier schematic and principle [Kes05] . . . . .	9
2.11.	Transfer function of an ideal, 3-bit ADC (redrawn from [LV02]) . . . . .	10
2.12.	Quantization noise as function of time (redrawn from [Kes05]) . . . . .	11
2.13.	Offset and Gain Error in the ADC characteristic. Notice the difference between the ideal, dotted line . . . . .	12
2.14.	Edge-Coupled Coplanar Waveguide . . . . .	14
2.15.	Coplanar Waveguide with Ground . . . . .	15
3.1.	General schema of KAPTURE-2 (cf. [CAB <sup>+</sup> 17, p.2]) . . . . .	17
3.2.	Signal with sample points . . . . .	18
3.3.	Photo of KAPTURE with highlighted main components. [Bro20, p. 61] . . . . .	18
3.4.	General schema of THERESA. For presentation purposes only four channels are shown. . . . .	19
3.5.	ZCU216 evaluation board . . . . .	20
3.6.	RFSoC block diagram . . . . .	20
3.7.	Track-And-Hold Timing diagram . . . . .	21
3.8.	CLK104 Add-on board clocking scheme . . . . .	22
3.9.	Clocking scheme on front-end card . . . . .	22
3.10.	Placeholder . . . . .	23
3.11.	Polaris Solver . . . . .	24
3.12.	Test Graph . . . . .	24
3.13.	Placeholder . . . . .	25
4.1.	RF DC Evaluation Tool architecture [Xil20a] . . . . .	27
4.2.	RF DC Evaluation Tool GUI [Xil20a] . . . . .	27
4.3.	Placeholder . . . . .	28
4.4.	Placeholder . . . . .	28
5.1.	wow . . . . .	29



# List of Tables

2.1. KARA characteristics . . . . .	5
3.1. Power consumption of components on the board . . . . .	23



# List of abbreviations

<b>KIT</b>	Karlsruhe Institute of Technology
<b>IPE</b>	Institut für Prozessdatenverarbeitung und Elektronik
<b>KARA</b>	Karlsruhe Research Accelerator
<b>KAPTURE</b>	Karlsruhe Pulse Taking Ultra-fast Readout Electronics
<b>CSR</b>	Coherent Synchrotron Radiation
<b>EO</b>	Electro-Optic
<b>ADC</b>	Analog-To-Digital-Converter
<b>SHA</b>	Sample-And-Hold-Amplifier
<b>THA</b>	Track-And-Hold-Amplifier
<b>PLL</b>	Phase-Locked-Loop
<b>FMC</b>	FPGA Mezzanine Card
<b>LVCMOS</b>	Low voltage complementary metal oxide semiconductor
<b>LVDS</b>	Low-voltage differential signaling
<b>LVPECL</b>	Low-voltage positive emitter-coupled logic
<b>PCIe</b>	PCI Express
<b>THERESA</b>	Terahertz Readout Sampling
<b>RFSoC</b>	Radio-Frequency System-On-Chip

# 1. Introduction

- Microbunching instabilities → THz radiation → Potential source of brilliant radiation
- Need to be studied to be able to control it
- Time-resolution critical, as instabilities at high frequency
- EO techniques to measure such signals
- Concept: combine time-stretch with FPGA → THERESA (**TeraHertz Readout Sampling**)



## 2. Theoretical Fundamentals

### 2.1. Coherent Synchrotron Radiation

Synchrotron radiation (SR) is produced in synchrotron radiation facilities (like electron storage rings) by accelerating relativistic electrons. Emission of SR occurs, when bending/deflecting the electrons in dipole magnets or undulators<sup>1</sup>.

Figure 2.1 shows a general scheme of an electron storage ring. Electrons, or rather electron bunches, are generated with an electron gun and are accelerated to almost speed of light by a linear accelerator (LINAC). The bunches are injected into the storage ring, after reaching their nominal energy in a booster. In the ring, the path of the electron bunches is altered by bending magnets, leading them on a circular trajectory. Due to emission of SR at each bending, the electrons lose energy, which has to be compensated. This is done in an accelerating radiofrequency (RF) cavity. Not shown in the scheme are the beamlines, which lead the SR radiation, or rather chosen wavelength regions of it, through an optical system to the respective user experiments.[Rou14] [Rot18]

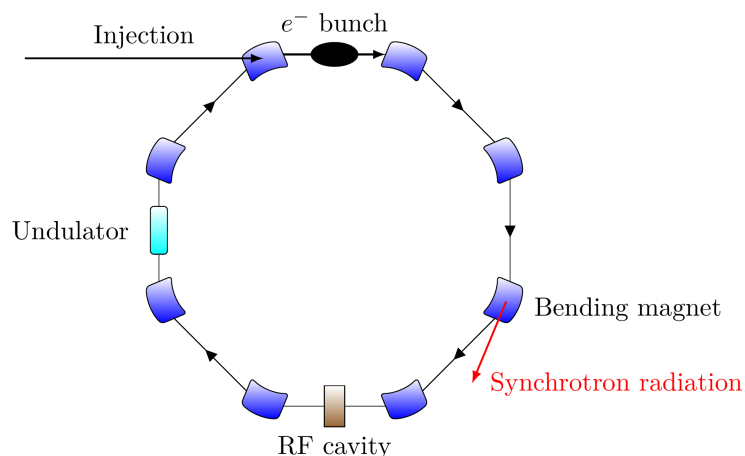


**Figure 2.1.:** Basic scheme of an electron storage ring (redrawn from [Rou14])

The range of SR reaches from hard X-rays down to the infrared region of the electromagnetic spectrum (see Figure 2.2). In contrast to other sources, it has properties like:

- high intensity
- high collimation
- polarisation
- well-defined timing of pulses

<sup>1</sup>Undulators are used to make the electrons oscillate by generating a periodic magnetic field

Due to this properties, synchrotrons are used for microscopy, spectroscopy, and time-resolved experiments in such fields like condensed matter physics, biology, material science and many more.

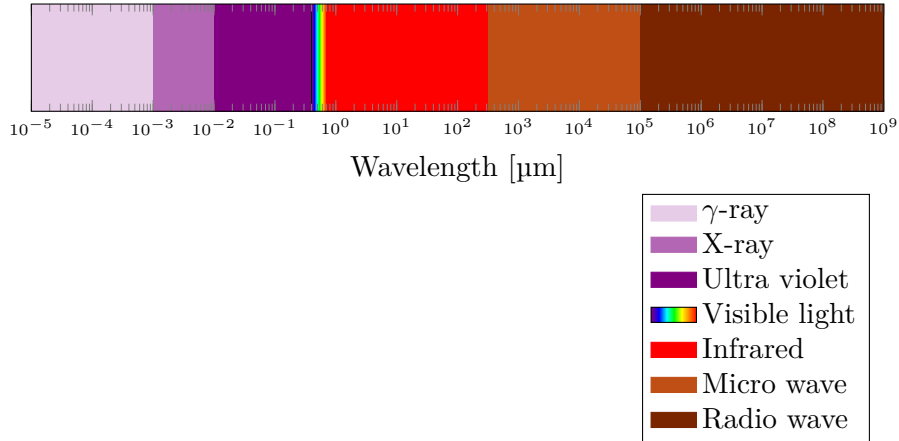


**Figure 2.2.:** Electromagnetic spectrum

### 2.1.1. Micro-Bunching Instabilities

Increasing demands in current and future accelerators call for higher brilliance of the emitted radiation. This is achieved by increased photon flux and reduction of the transverse emittance. For longitudinal coherence, the electron bunches are shortened, which results in emission of coherent synchrotron radiation (CSR) at frequencies up to the THz range. However, this introduces complex dynamics, as the electrons interact with their own radiation. This manifests into the so called micro-bunching instability: the formation of microstructures (in the sub-millimetre to centimetre range) in the longitudinal density profile of the electron bunches. Being on the one side a limitation to the stable operation of the overall system at high current density/short bunch length mode. On the other side, these instabilities can be potential sources of brilliant THz radiation. A thorough understanding of these dynamics is necessary to control the emission in this spectral domain which enables usage in experiments. [Rot18] [Bro20]

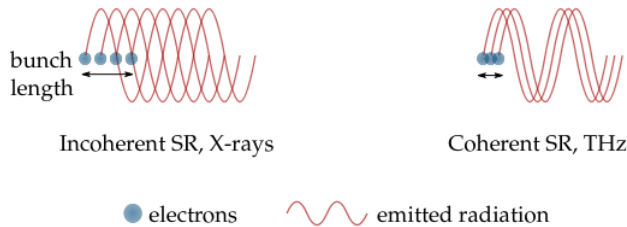


**Figure 2.3.:** Placeholder [Rot18]

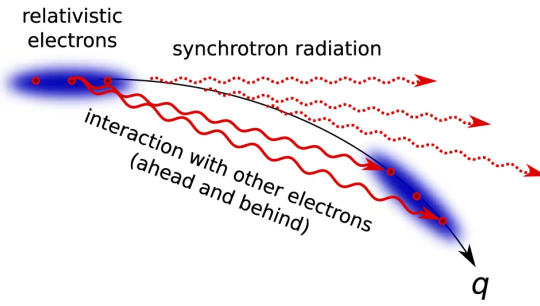


**Figure 2.4.:** Electrons interact with their own radiation [BBB<sup>+</sup>19]

## KARA

- Located at the Karlsruhe Institute of Technology (KIT)
- Up to 184 electron packages (bunches) can be filled with a distance of 2 ns (500 MHz) between two adjacent bunches
- Operated by the Institute of Beam Physics and Technology (IBPT)
- Microtron, Booster Synchrotron, and Storage Ring

**Table 2.1.:** KARA characteristics

Beam energy	2.5 GeV
Circumference	110 m
RF frequency	499.7 MHz
Harmonic number	184
Number of RF stations	2
Number of cavities per station	2
Accelerating voltage	1.4 MeV

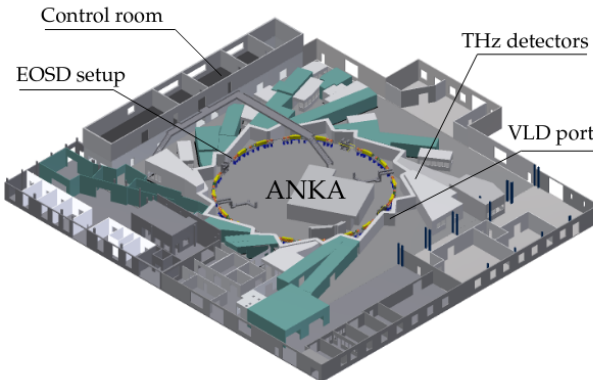


**Figure 2.5.:** Facility [Rot18]

## 2.2. Electro-Optic Techniques and Time-Stretch

Several Electro-Optic (EO) techniques exist, to measure THz radiation with a sub-picosecond resolution. In this section, the techniques used in storage rings and the time-stretch technique are presented.

### 2.2.1. Scanning-Type Electro-Optic Sampling

A short laser pulse (duration typically hundreds of femtoseconds) co-propagates with a THz pulse from CSR (range of picoseconds) in an electro-optical crystal. Due to the Pockels effect<sup>2</sup> the THz pulse causes a time dependent birefringence in the crystal. This modulates the polarization of the laser pulse. To sample the pulse, the delay between the laser and the THz pulse is varied. To detect the changing polarization, the polarization of the laser pulse is transformed in an intensity modulation. A general scheme of the system is shown in Figure 2.6. For this technique a stable emission of the THz pulses is crucial, as they are not measured in one acquisition. [Rou14]

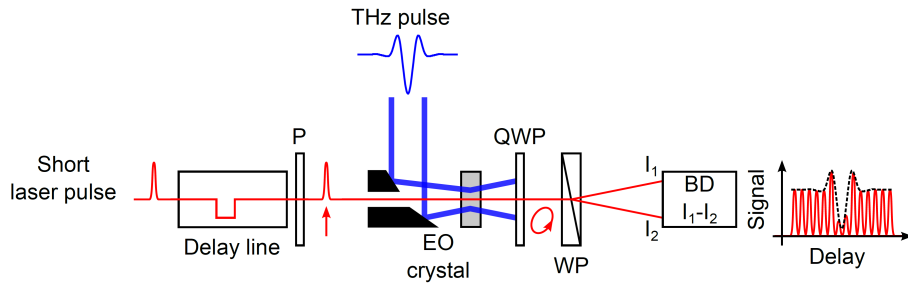


**Figure 2.6.:** Scheme of Scanning-Type Electro-Optical Sampling System [Rou14]

### 2.2.2. Spectrally Resolved Electro-Optic Detection

In contrast to the EOS, single-acquisition is possible with the spectrally resolved electro-optic detection technique. The short laser pulse is first stretched to a duration similar to the Thz pulse in a dispersive material (stretcher). In this way the pulse is chirped, meaning the instantaneous frequency of the pulse varies over time. Together with the THz the laser pulse propagates in a EO crystal. Again, the induced birefringence modulates the laser pulse, not only in time, but also in the optical spectrum. The polarization state of the pulse is converted into an amplitude/intensity modulation. To retrieve the THz pulse shape in time, the spectrum of the laser pulse is measured with a spectrometer. A general scheme of the system is shown in Figure 2.7. [Rou14]

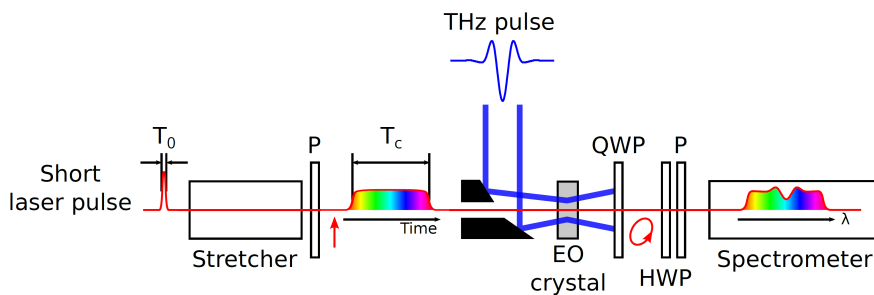


**Figure 2.7.:** Scheme of Spectrally Encoded Electro-Optical Detection System [Rou14]

<sup>2</sup>"The Pockels effect is the name given to the occurrence of birefringence and to the change in existing birefringence phenomena in an electric field linearly proportional to the electric field strength." [Gmb]

The temporal resolution of this method is limited due to a finite chirp rate

$$\text{chirp rate} = \frac{\text{laser bandwidth}}{\text{laser pulse duration after stretcher}}. \quad (2.1)$$

The resolution  $T_{\min}$  is determined as

$$T_{\min} = \sqrt{T_0 T_c} \quad (2.2)$$

with the bandwidth-limited pulse duration (before stretcher)  $T_0$  and the duration of the chirped laser pulse  $T_c$ .

### 2.2.3. Photonic Time-Stretch Technique

The working principle of the optic time-stretch technique can be described in two steps (see Figure 2.8). First, like in the EOSD before, a short laser pulse is propagated in a dispersive medium (optical fiber of length  $L_1$ ). This results in a chirped laser pulse of the duration

$$T_1 = \Delta\lambda D_1 L_1 \quad (2.3)$$

with the optical bandwidth of the laser pulse  $\Delta\lambda$  and the dispersion parameter  $D_1$  of the fiber. The next step is the time-to-wavelength-mapping where a temporal intensity modulation is imprinted on the chirped pulse. After that, the modulated chirped pulse propagates through another dispersive medium, a fiber of the length  $L_2$ . In this way, the temporal modulation of the pulse is further stretched to the duration  $T_2$ , which is long enough for detection with photodetectors. [Rou14] The factor, by which the pulse is slowed down, is calculated as:

$$M = 1 + \frac{L_1}{L_2} \quad (2.4)$$

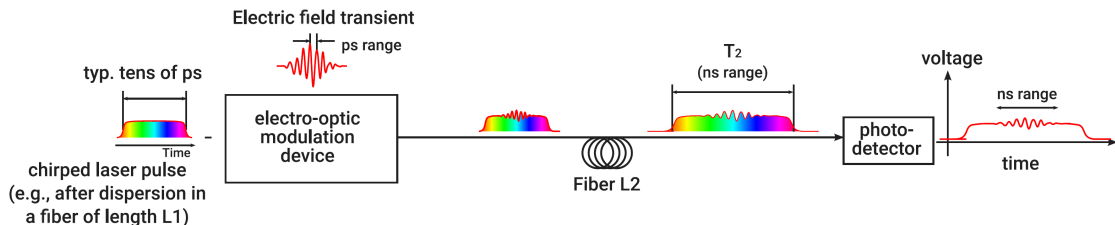


**Figure 2.8.:** Electro-Optical Time-Stretch Technique [SELP<sup>+</sup>16]

### 2.2.4. Time-Stretched Spectrally-Encoded Electro-Optic detection

## 2.3. Analog-To-Digital Converters

The following section aims to recapitulate the theory and characteristics concerning Analog-To-Digital-Converters (ADCs).

### 2.3.1. Sampling Theory

An ADC samples an analog signal with a frequency  $f_s$ . This frequency has to be chosen in such way, that the original signal can be fully reconstructed. The *Nyquist criteria* states, that in order to accurately represent a bandlimited, continuous signal

$$y(t) \circlearrowleft Y(f) \quad \text{with} \quad Y(f) = 0, |f| \geq \frac{B}{2} \quad (2.5)$$

it has to be sampled with a frequency  $f_s$  respecting

$$f_s \geq B \quad \text{or} \quad f_s \geq 2f_a \quad (2.6)$$

with  $f_a$  being the highest frequency contained in the signal. [Kes05] [Pue15]

In other words,  $f_a$  must be inside of the *Nyquist bandwidth*, which is the spectrum from DC to  $f_s/2$ . Violation of this rule leads to *aliasing*.

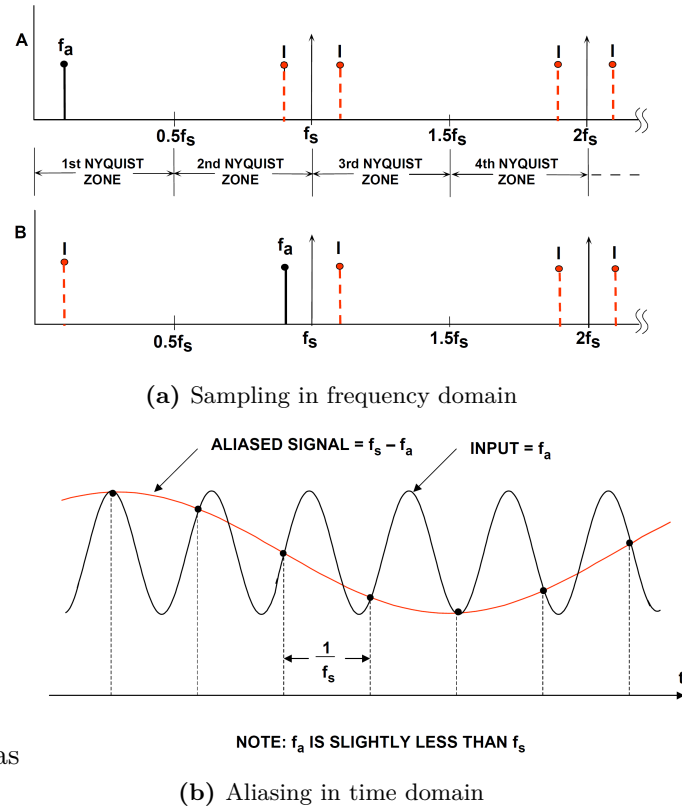
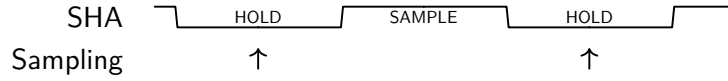


**Figure 2.9.:** Analog signal with frequency  $f_a$  sampled at  $f_s$  respecting (A) and not respecting (B) the Nyquist criteria. Figure 2.9b shows the effect of case B in time domain. [Kes05]

### Sample-And-Hold-Amplifier

ADCs need a certain amount of time to sample the input signal. If the value of the signal changes by more than one Least-Significant-Bit (LSB) during this period, this can result in large errors in the output signal. Therefore, so called Sample-And-Hold-Amplifiers (SHA)

are used in front of ADCs to hold the input value for the needed amount of time. The ADC sampling time needs to be timed in such way, that the analog-to-digital conversion falls into the hold period of the SHA and doesn't exceed into the sample period, for example like shown schematically in the diagram below. Thus, the upper frequency limitation is not determined by the ADC itself, but rather by the aperture jitter, bandwidth, distortion, etc. of the SHA. [Kes05]



In addition to the SHA, there is also the Track-And-Hold-Amplifier (THA). Instead of a sample period, the THA has a track period, where the output of the amplifier tracks the input signal (see also Figure 2.10). When switching to hold mode, the signal at this instant is held. This is opposed to the SHA, where the output during sample mode is actually not defined and is set to the value of the input signal, only when switching into hold mode.

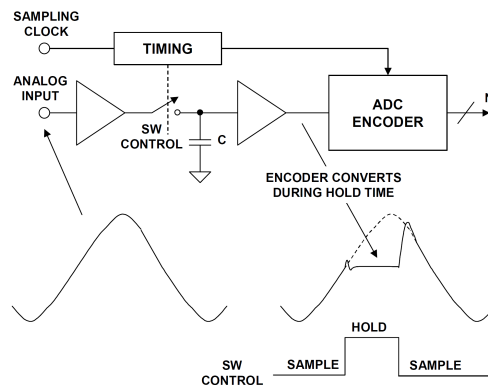


**Figure 2.10.:** Track-And-Hold-Amplifier schematic and principle [Kes05]

### 2.3.2. Characteristics of Analog-To-Digital-Converters

ADCs are used to translate analog quantities into digital signals, which can be processed by information processing, computing, data transmission and control systems. The translation can be seen as encoding a continuous-time analog input (voltage) into a series of discrete, N-bit words. This can be expressed as

$$V_{\text{IN}} = V_{\text{FS}} \sum_{k=0}^{N-1} \frac{b_k}{2^{k+1}} + \epsilon \quad (2.7)$$

with  $V_{\text{IN}}$  being the input voltage,  $V_{\text{FS}}$  the full-scale voltage,  $b_k$  the individual output bits and  $\epsilon$  the quantization error. Figure 2.11 shows the ideal transfer function of a 3-bit ADC.

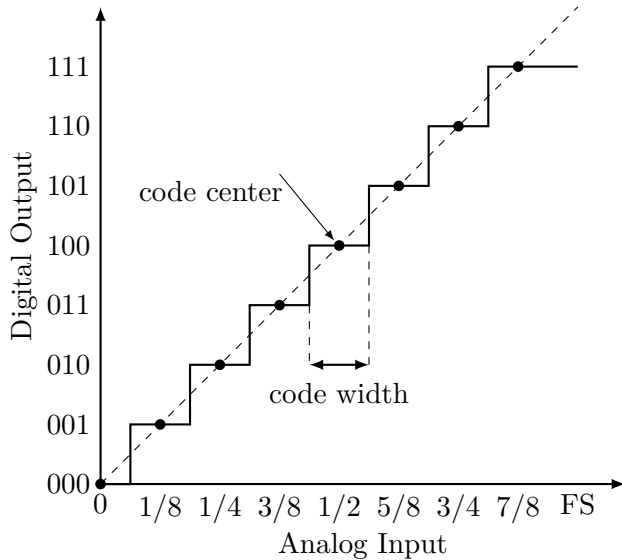


**Figure 2.11.:** Transfer function of an ideal, 3-bit ADC (redrawn from [LV02])

For an ideal converter, the number of bits would be sufficient to fully characterize it. Real ADCs however differ from the ideal behaviour, introducing static and dynamic imperfections. Different applications have different requirements, which leads to a number of specifications. These can be divided into three categories [LV02]:

- Static parameters
- Frequency-domain dynamic parameters
- Time-domain dynamic parameters

This section provides an overview of these figures of merit. Which of these are needed to specify the necessary performance of the ADC has to be chosen for each application accordingly.

### 2.3.2.1. Quantization Noise

Even in an ideal N-bit converter there will be errors during the quantization, which behave like noise. The reason is that each N-bit word represents a certain range of analog input values, which is 1 LSB wide (*code width*) and centered around a *code center* (see Figure 2.11) [LV02]. The input voltage is always assigned to the word of the nearest code center. This means that there will always be a difference between the code center and the actual input. The difference between the corresponding voltage of the respective code center and the analog input is called the *quantization error*. For an equidistant quantization it is

$$|e_q(t)| = |x(t) - x_q(t)| \leq \frac{q}{2} \quad (2.8)$$

with  $x_q(t)$  being the quantized/discrete signal,  $x(t)$  the input signal and  $q$  the width of the quantization stage. [Pue15]

Assuming the error voltage uncorrelated and uniformly distributed, the theoretical (maximum) Signal-To-Noise-Ratio (SNR) of this *quantization noise* can be calculated. In the time domain, the quantization error can be approximated with a sawtooth signal:

$$e(t) = st, \quad -\frac{q}{2s} < t < \frac{q}{2s} \quad (2.9)$$

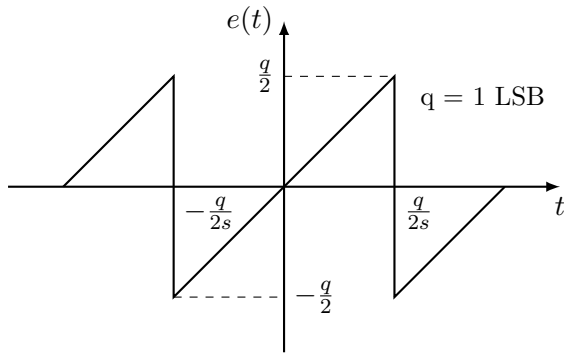


**Figure 2.12.:** Quantization noise as function of time (redrawn from [Kes05])

The power of the quantization noise, which is assumed to be uncorrelated and broadband, can be calculated as the mean-square of  $e(t)$ :

$$P_{QN} = e_{\text{rms}}^2 = \overline{e^2(t)} = \frac{s}{q} \int_{-q/2s}^{+q/2s} (st)^2 dt = \frac{s^3}{q} \left[ \frac{t^3}{3} \right]_{-\frac{q}{2s}}^{+\frac{q}{2s}} = \frac{q^2}{12} \quad (2.10)$$

To calculate the maximal SNR of an ideal converter, a full-scale input sine wave is assumed:

$$u(t) = u_s \sin(2\pi ft) = \frac{2^N q}{2} \sin(2\pi ft) = 2^{N-1} q \sin(2\pi ft) \quad (2.11)$$

With the effective value of the signal amplitude

$$u_{\text{eff}} = \frac{u_s}{\sqrt{2}} = \frac{2^{N-1} q}{\sqrt{2}} \quad (2.12)$$

and the quantization noise power, the SNR can be calculated as

$$\text{SNR} = \frac{P_{\text{signal}}}{P_{\text{noise}}} = \frac{u_{\text{eff}}^2}{e_{\text{rms}}^2} = \frac{2^{2N-2} q^2 / 2}{q^2 / 12} = 2^{2N} \cdot 1.5. \quad (2.13)$$

In decibel:

$$\text{SNR|}_{\text{dB}} = 10 \log (2^{2N} \cdot 1.5) = 6.02N + 1.76 \quad (2.14)$$

[Pue15] [Kes05]

### 2.3.2.2. Static parameters

*Static parameters* are specifications, which can be measured at low speed/DC.

#### Accuracy

*Accuracy* is the total error at a known voltage, which includes:

- Quantization error
- Gain error
- Offset error
- Nonlinearities

#### Resolution

*Resolution* is the number of bits  $N$  of the ADC. Depending from the resolution are the size of the LSB, which in its turn determines the dynamic range, code widths and quantization error.

## Dynamic Range

Ratio between smallest possible output (LSB voltage) and the largest possible output (full-scale voltage). It can be calculated as

$$20 \log 2^N \approx 6N \quad (2.15)$$

## Offset and Gain Error

The *offset error* is the deviation of the first transition voltage from the ideal  $1/2$  LSB. *Gain Error* defines the deviation of the slope of the line going through the zero and full-scale point of the transfer function. These errors can easily be corrected by calibration. Refer to Figure 2.13

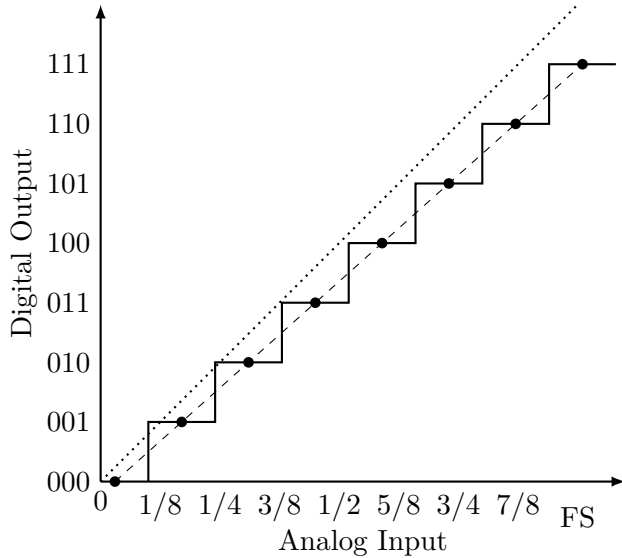


**Figure 2.13.:** Offset and Gain Error in the ADC characteristic. Notice the difference between the ideal, dotted line

## Integral and Differential Nonlinearity Distortion

*Integral nonlinearity* in the transfer function of data converters results from the integral nonlinearities of the front-end, SHA and also the ADC itself. These nonlinearities depend on the input signal amplitude. distance of the code centers in the A/D converter characteristic from the ideal line *Differential nonlinearities* stem exclusively from the encoding process in the ADC. They not only depend on the input signal amplitude, but also on the positioning along the transfer function. The deviation of the code transition widths from the ideal width of 1 LSB

### 2.3.2.3. Dynamic performance

#### Frequency-Domain

- SINAD
- ENOB
- SFDR
- Total Harmonic Distortion
- Intermodulation Distortion

- Effective Resolution Bandwidth
- Full-Power Bandwidth
- Full-Linear Bandwidth

### Time-Domain

- Aperture Delay
- Aperture Jitter
- Transient Response
- Overvoltage Recovery

In an ADC (with built-in SHA) there are a couple of sources, which introduce noise and distortion:

- **Input Stage:** Wideband noise, nonlinearity and bandwidth limitation
- **SHA:** Nonlinearity, aperture jitter<sup>3</sup> and bandwidth limitation
- **ADC:** Quantization noise, integral and differential nonlinearity

In the following the most important specifications are described, which are used to characterize the performance of ADCs.

### Equivalent Input Referred Noise

Internal circuits of wideband ADCs produce rms noise due to resistor and thermal ("kT/C") noise, which is also present for DC signals. Therefore, the output of the ADC is a distribution of codes which is centered around the value of a DC input. For measuring the value of the noise, the ADC input is grounded, or held at a specific DC value, and a large amount of samples is collected and plotted as a histogram. The noise is approximately Gaussian, thus the standard deviation can easily be calculated.

### Noise-Free Code Resolution

The input referred noise described above determines the *noise-free code resolution*, which is the number of bits, beyond which it is not possible to resolve individual codes. [Kes05]

#### 2.3.3. Interleaving

- Net sample rate
- Interleaving Spurs

[MR15]

---

<sup>3</sup>Aperture jitter is the sample-to-sample variation in aperture delay, with *aperture delay* meaning the time, which is needed by the SHA to disconnect the holding capacitor from the input buffer.

## 2.4. RF/Microwave Design Basics

### 2.4.1. General Techniques/Strategies?

### 2.4.2. Coplanar Waveguides

#### Surface Coplanar Waveguide with Ground

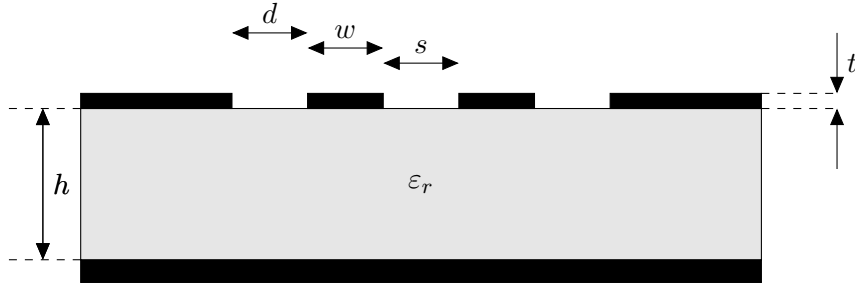


**Figure 2.14.:** Edge-Coupled Coplanar Waveguide

The corresponding equations are [Wad91, p197-198]:

$$Z_{0,o} = \frac{\eta_0}{\sqrt{\epsilon_{eff,o}}} \left( \frac{1.0}{2.0 \frac{K(k_o)}{K'(k_o)} + \frac{K(\beta_1)}{K'(\beta_1)}} \right) \quad (2.16)$$

$$Z_{0,e} = \frac{\eta_0}{\sqrt{\epsilon_{eff,e}}} \left( \frac{1.0}{2.0 \frac{K(k_e)}{K'(k_e)} + \frac{K(\beta_1 k_1)}{K'(\beta_1 k_1)}} \right) \quad (2.17)$$

$$\epsilon_{eff,o} = \frac{2.0 \epsilon_r \frac{K(k_o)}{K'(k_o)} + \frac{K(\beta_1)}{K'(\beta_1)}}{2.0 \frac{K(k_o)}{K'(k_o)} + \frac{K(\beta_1)}{K'(\beta_1)}} \quad (2.18)$$

$$\epsilon_{eff,e} = \frac{2.0 \epsilon_r \frac{K(k_e)}{K'(k_e)} + \frac{K(\beta_1 k_1)}{K'(\beta_1 k_1)}}{2.0 \frac{K(k_e)}{K'(k_e)} + \frac{K(\beta_1 k_1)}{K'(\beta_1 k_1)}} \quad (2.19)$$

Where

$$k_o = \Lambda \frac{-\sqrt{\Lambda^2 - t_c^2} + \sqrt{\Lambda^2 - t_B^2}}{t_B \sqrt{\Lambda^2 - t_c^2} + t_c \sqrt{\Lambda^2 - t_B^2}} \quad (2.20)$$

$$k_e = \Lambda' \frac{-\sqrt{\Lambda'^2 - t_c'^2} + \sqrt{\Lambda'^2 - t_B'^2}}{t_B' \sqrt{\Lambda'^2 - t_c'^2} + t_c' \sqrt{\Lambda'^2 - t_B'^2}} \quad (2.21)$$

$$\Lambda = \frac{\sinh^2 \left( \frac{\pi(s/2.0+w+d)}{2.0h} \right)}{2} \quad (2.22)$$

$$t_c = \sinh^2 \left( \frac{\pi(s/2.0+w)}{2.0h} \right) - \Lambda \quad (2.23)$$

$$t_B = \sinh^2 \left( \frac{\pi s}{4.0h} \right) - \Lambda \quad (2.24)$$

$$\Lambda' = \frac{\cosh^2\left(\frac{\pi(s/2.0+w+d)}{2.0h}\right)}{2} \quad (2.25)$$

$$t'_c = \sinh^2\left(\frac{\pi(s/2.0+w)}{2.0h}\right) - \Lambda' + 1.0 \quad (2.26)$$

$$t'_B = \sinh^2\left(\frac{\pi s}{4.0h}\right) - \Lambda + 1.0 \quad (2.27)$$

The parameters have to be chosen according to

$$s + 2.0w + 2.0d \leq h \quad (2.28)$$

to guarantee coplanar propagation. [Wad91]

### Surface Coplanar Waveguide with Ground

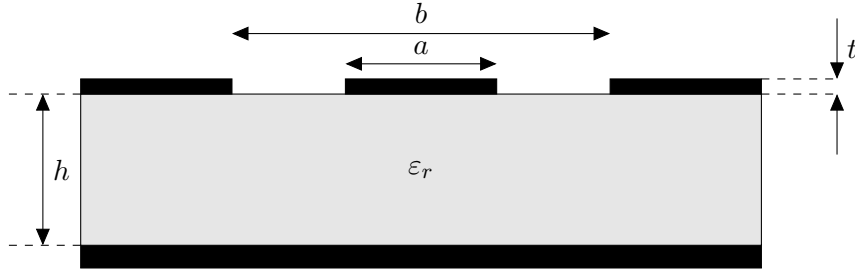


**Figure 2.15.:** Coplanar Waveguide with Ground

The characteristic impedance of a coplanar waveguide is given as follows [Wad91]:

$$Z_0 = \frac{60.0\pi}{\sqrt{\epsilon_{eff}}} \frac{1.0}{\frac{K(k)}{K(k')} + \frac{K(k_1)}{K(k'_1)}} \quad (2.29)$$

It comprises of the following components, with  $K(k)$  being an elliptical integral of the first kind (see also [BSMM99, p. 430]):

$$k = a/b \quad (2.30)$$

$$k' = \sqrt{1.0 - k^2} \quad (2.31)$$

$$k'_1 = \sqrt{1.0 - k_1^2} \quad (2.32)$$

$$k_1 = \frac{\tanh(\frac{\pi a}{4.0h})}{\tanh(\frac{\pi b}{4.0h})} \quad (2.33)$$

$$\epsilon_{eff} = \frac{1.0 + \epsilon_r \frac{K(k')}{K(k)} \frac{K(k_1)}{K(k'_1)}}{1.0 + \frac{K(k')}{K(k)} \frac{K(k_1)}{K(k'_1)}} \quad (2.34)$$



### 3. Design and Development of the System

This chapter covers the architecture and design of the system.

#### 3.1. General architecture

In this section the general architecture of the THERESA system is described. The idea for the new system is to reuse the concept of the already existing sampling system KAPTURE (**K**arlsruhe **P**ulse **T**aking **U**ltra-fast **R**eadout **E**lectronics), which is using four ADCs, and expanding it to 16. Therefore, also the architecture of the latter is explained briefly.

##### 3.1.1. KAPTURE-2

KAPTURE, which was developed at IPE, is a system designed to continuously sample ultra-short pulses generated by Terahertz detectors. It consists of a daughter card, holding four sampling channels, mounted on a FPGA . The FPGA is connected to a computer via PCIe for further processing of the acquired data. [Bro20] The newer version, KAPTURE-2, was designed for more accurate sampling for pulse repetition rates up to 2 GHz. The acquired data is processed with a FPGA and GPU architecture. [CAB<sup>+</sup>17]

The general structure of the board is shown in Figure 3.1.

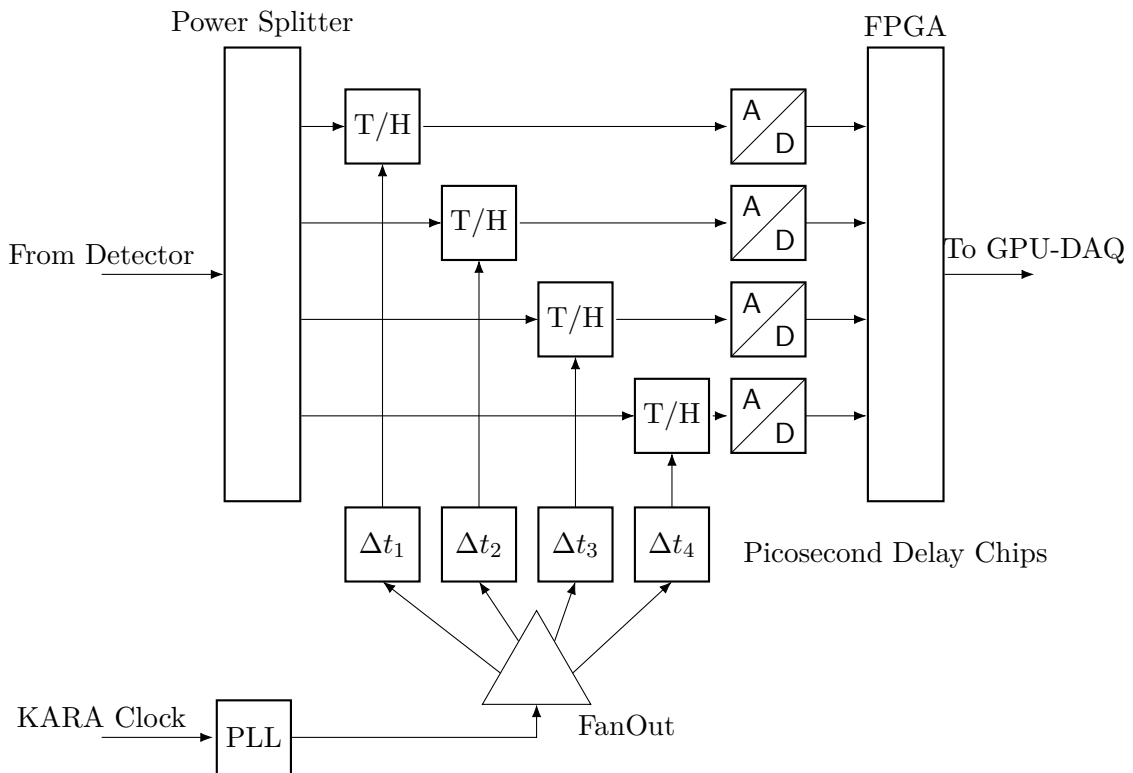


**Figure 3.1.:** General schema of KAPTURE-2 (cf. [CAB<sup>+</sup>17, p.2])

The pulse from the THz detector is fed into a power splitter, which splits the signal into four identical pulses and distributes them to four channels, consisting of a respective Track-And-Hold-Amplifier (THA) unit and a 12-bit ADC@500 MS/s. The sampling time of each unit can be adjusted individually with a Picosecond Delay Chip with a resolution of 3 ps (maximal delay range: 100 ps). The clock signal is provided by KARA, which is cleared from jitter by a Phase-Locked-Loop (PLL). This ensures the synchronization of the ADCs with the RF system. The clean clock signal is distributed to the delay chips via fan-out. [CAB<sup>+</sup>17]

The resulting sampling of the detector signal is shown Figure 3.2 (simplified representation).

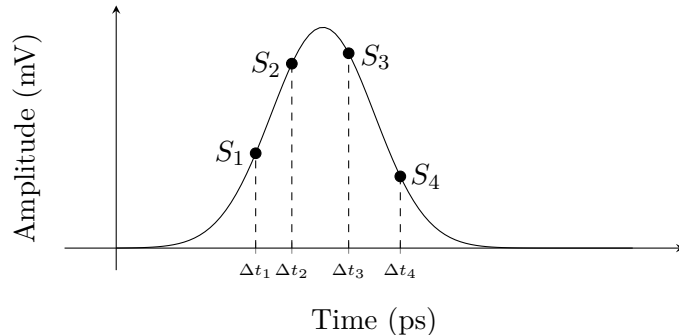


**Figure 3.2.:** Signal with sample points

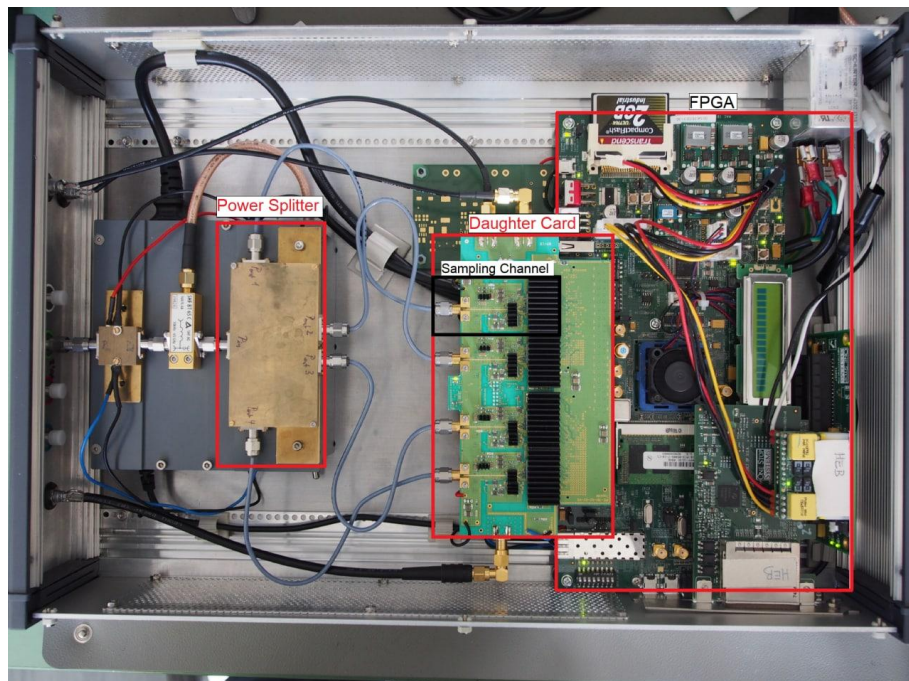


**Figure 3.3.:** Photo of KAPTURE with highlighted main components. [Bro20, p. 61]

### 3.1.2. New System THERESA

In principle, the new system has the same structure, as KAPTURE. Notable differences are firstly the number of ADCs, which is increased up to 16. Secondly, the latter are not located on the daughter card anymore, but inside the Xilinx Zynq UltraScale+ RFSoC ZU49DR on the ZCU216 Evaluation Kit on which the front-end card is mounted. Figure 3.4 shows the general schema of the sampling system, reduced to four channels for presentation purposes.

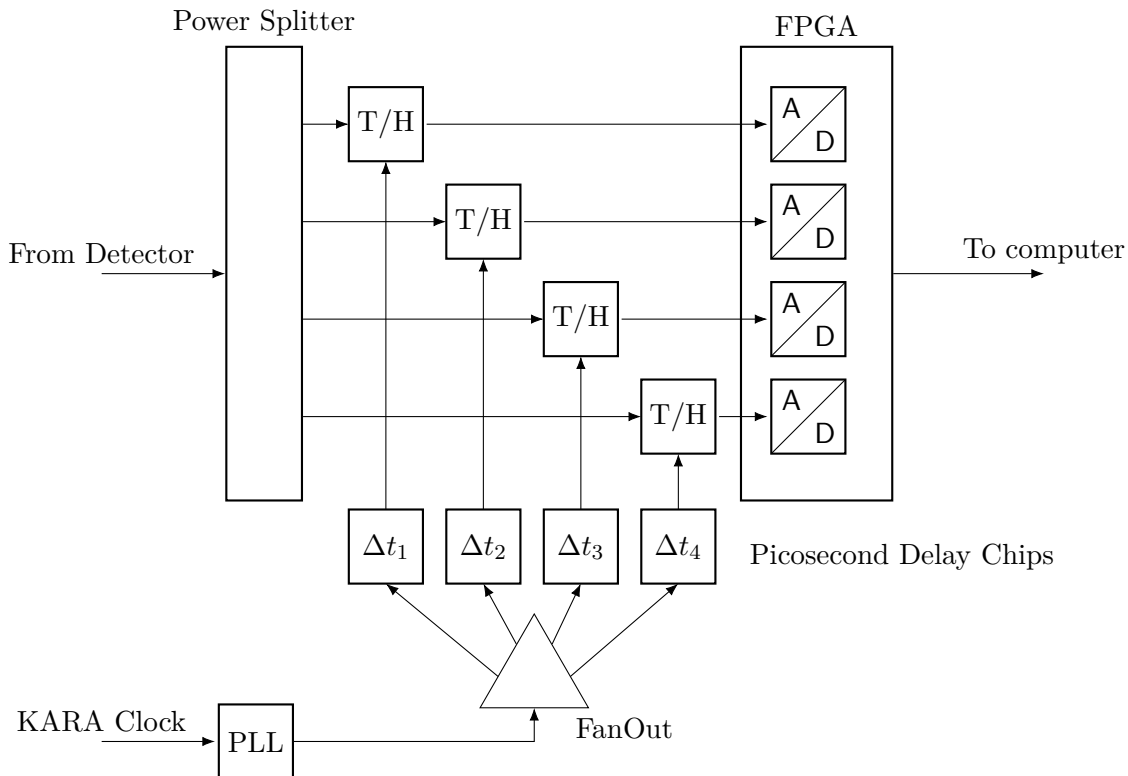
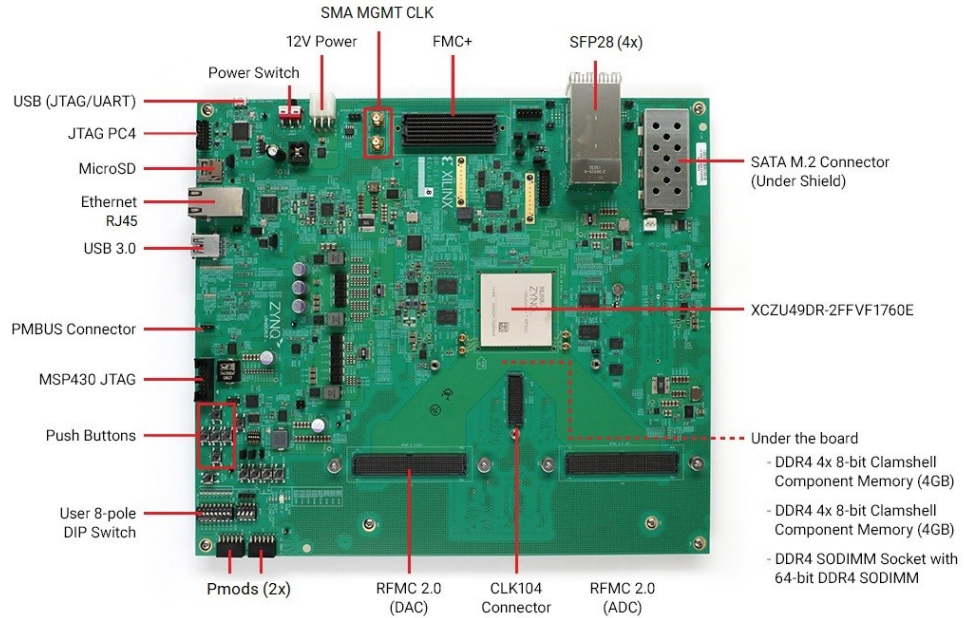


**Figure 3.4.:** General schema of THERESA. For presentation purposes only four channels are shown.

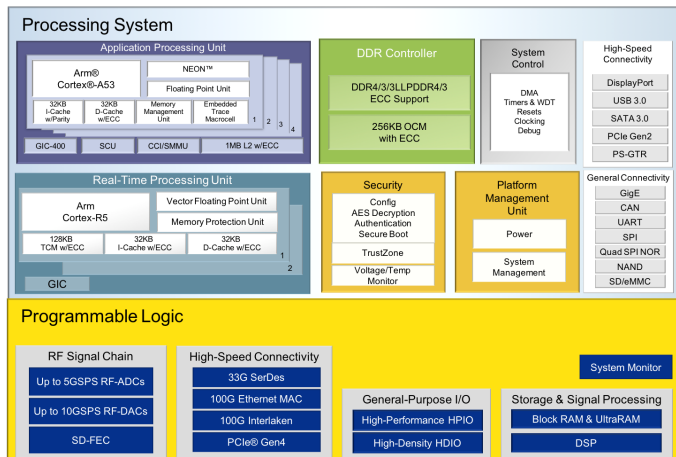
### Xilinx Zynq UltraScale+ RFSoC ZCU216 Evaluation Card

The card, holding the sampling channels, should be mounted on a ZCU216 evaluation board. This board is the newest generation of Xilinx' evaluation cards, which has features suitable for the purpose at hand.

- Sixteen 14-bit, 2.5GSPS RF-ADC
- Sixteen 14-bit, 10GSPS RF-DAC
- I/O expansion options – FPGA Mezzanine Card (FMC+) interfaces, RFMC 2.0 interfaces, and Pmod connections



**Figure 3.5.:** ZCU216 evaluation board

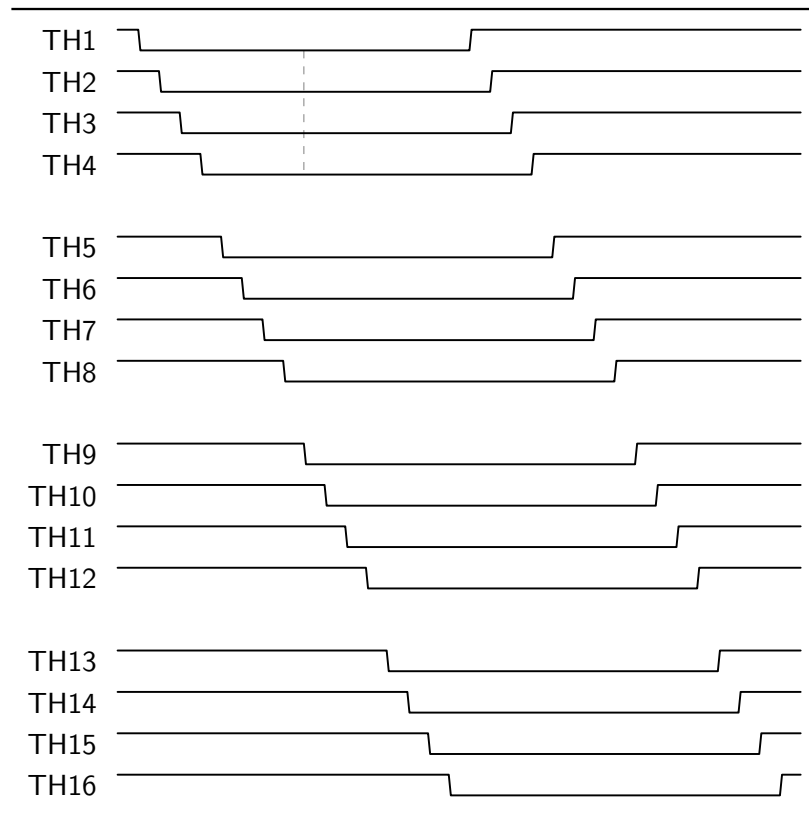


**Figure 3.6.:** RFSoC block diagram

### 3.1.3. Requirements

#### Step size delay chip

The necessary step size for the delay chips, when using 16 ADC@2 GS/s in time-interleaving mode, is:  $\frac{2 \text{ GS/s}}{16} = 31 \text{ ps}$

**Frequency**

**Figure 3.7.:** Track-And-Hold Timing diagram

**Data Rate****Visualization/GUI**

### 3.2. Design of the front-end card

In this section, the design of the front-end card is covered.

#### 3.2.1. Sampling-Channel

##### Track-And-Hold-Amplifier

Explain why better than Sample-And-Hold-Amplifier.

##### Delay Chip NB6L295

Dual Channel Programmable Delay Chip.

- Two individual variable delay channels
- Dual Delay: minimal delay 3.2 ns
- Total Delay Range: 3.2 ns to 8.8 ns per Delay Channel
- 11 ps Increments in 511 steps
- 100 ps Typical Rise and Fall Times

#### 3.2.2. Clocking

On Xilinx CLK104 add-on board the LMX2594 is used to generate additional, high-frequency clocks for the ADCs/DACs. → reuse in front-end card

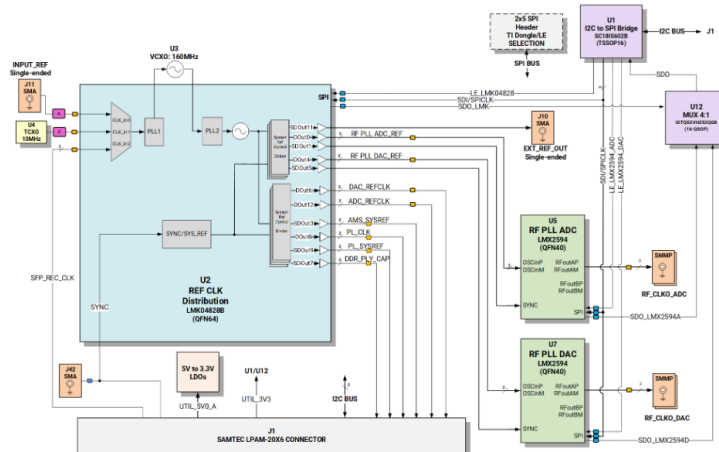


Figure 3.8.: CLK104 Add-on board clocking scheme

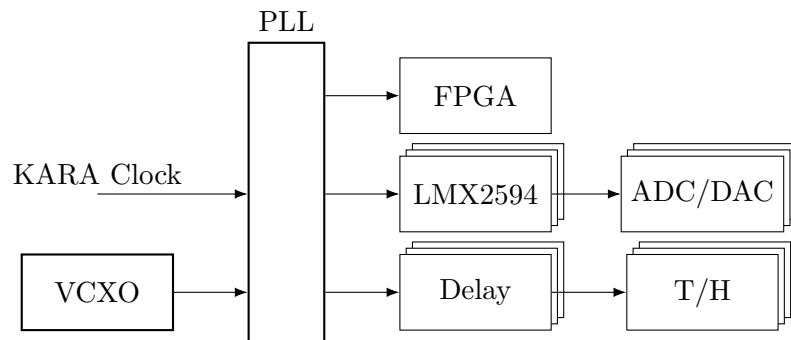


Figure 3.9.: Clocking scheme on front-end card

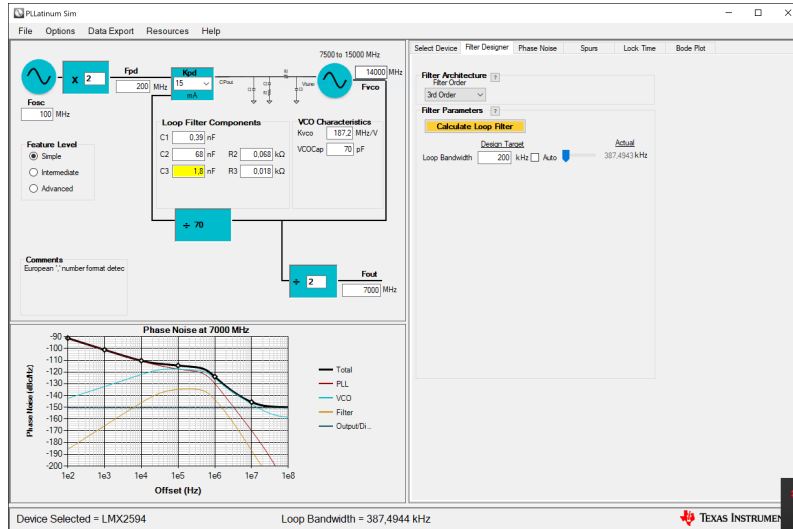


Figure 3.10.: Placeholder

### 3.2.3. Power Supply

For the Track-And-Hold amplifiers a new power supply unit – the ADP1741 (Analog Devices) – should be used. It is necessary to think about the amount of power supply chips needed. As a rule of thumb, the power supply should provide twice the maximum power needed by the components it drives. The power consumption/maximum current for the respective components on the THERESA board is listed in Table 3.1.

Table 3.1.: Power consumption of components on the board

Component	$V_{cc}$ (V)	$I_{max}$ (A)	$P_{max}$ (W)	#parts	$I_{tot}^1$ (A)
HMC5649 (T/H-Amplifier)	2	0.221	0.442	16	3.536
	-5	-0.242	1.21		3.872
HMC856 (Delay)	-3.3	0.185	-0.611	16	2.96
HMC987LP5E (Fan-Out)	3.3	0.234 <sup>2</sup>	0.772	2	0.468
LMC0480 (PLL)	3.3	0.590 <sup>3</sup>	1.947	1	0.590
VCXO	3.3	0.03	0.198	1	0.03

<sup>1</sup>for 16 ADCs<sup>2</sup>All Outputs and RF-Buffer<sup>3</sup>All CLKs

The maximal current which the ADP1741 can provide @2V is 2 A. This means, with one Track-And-Hold amplifier requiring a maximal current of 0.221 A, one ADP1741 can handle four units according to the rule mentioned beforehand ( $I_{max\_ADP1741} = 2 \text{ A} > 2 * I_{tot}, I_{tot} = 4 * 0.221 \text{ A} = 0.884 \text{ A}$ ).

### 3.3. PCB-Layout

#### 3.3.1. Floor Planning

#### 3.3.2. Transmission lines

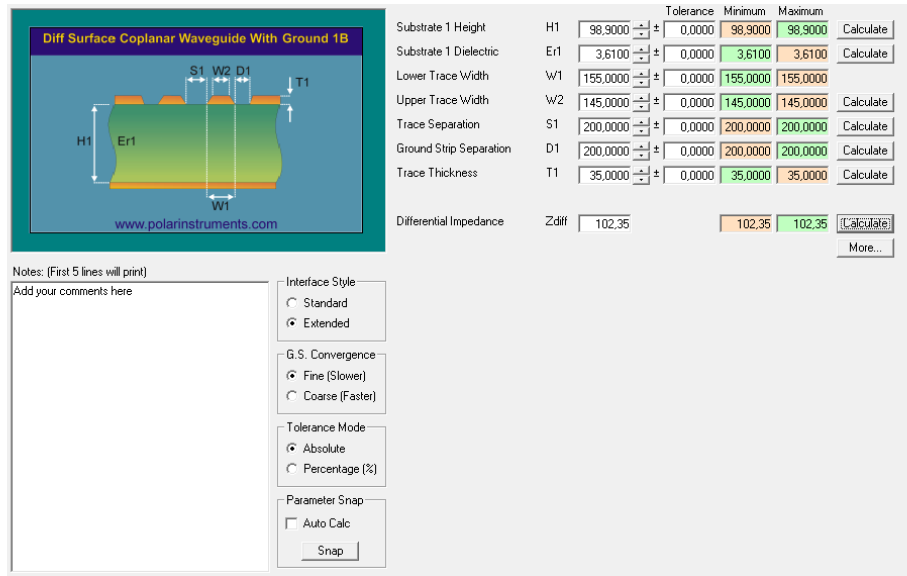


Figure 3.11.: Polaris Solver

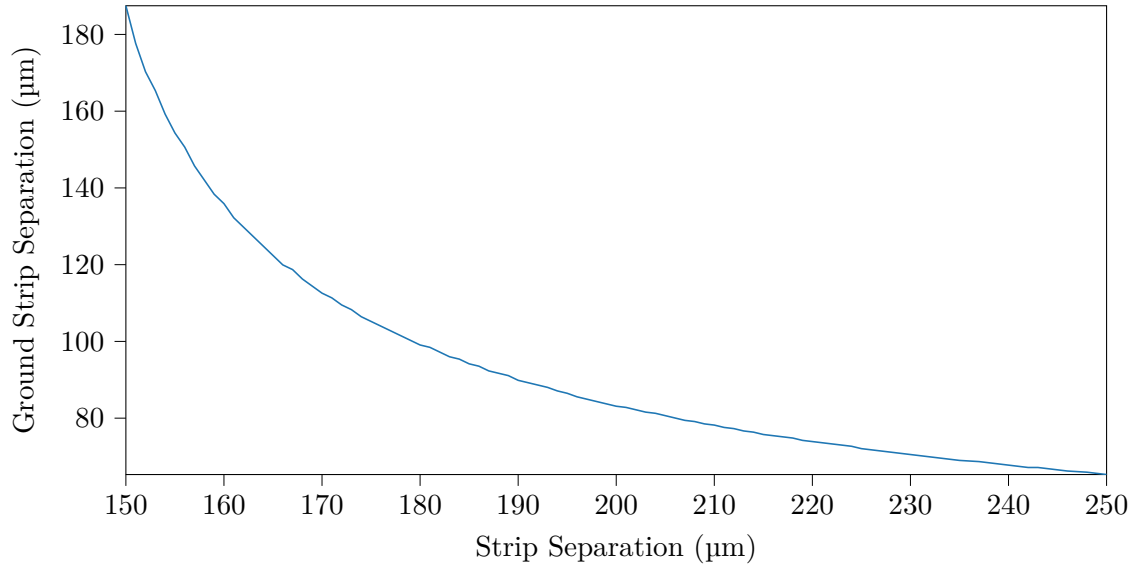


Figure 3.12.: Test Graph

### 3.4. Firmware

#### 3.4.1. General Design

##### 3.4.1.1. Firmware for Front-End Card

###### Clocking

###### SPI-Interface

##### 3.4.1.2. Data Capture

Figure 4: RF-ADC DDR Block Architecture for Quad RF-ADC Tiles

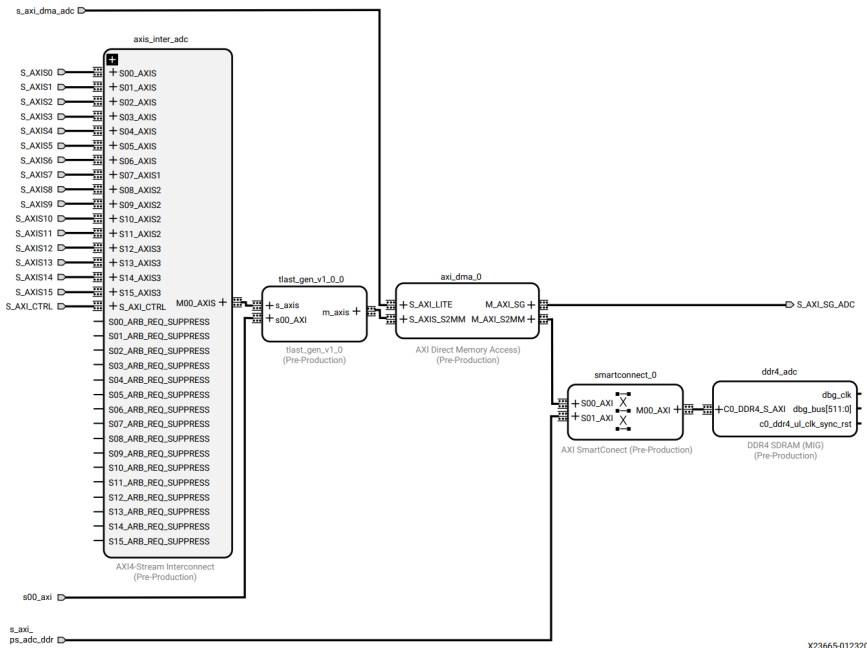


Figure 3.13.: Placeholder

##### 3.4.1.3. Visualization



## 4. Characterization

### 4.1. Evaluation of the ZCU216 Board/ADCs

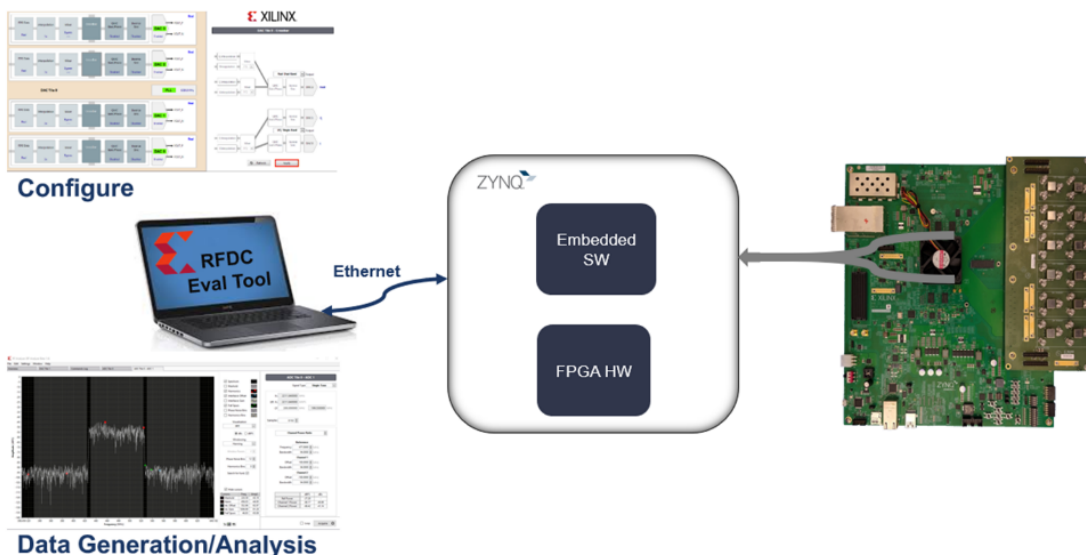


Figure 4.1.: RF DC Evaluation Tool architecture [Xil20a]

#### 4.1.1. Measurements with Xilinx XM655 add-on card

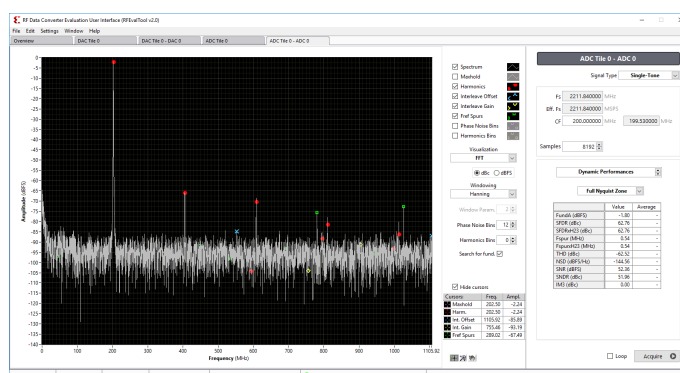
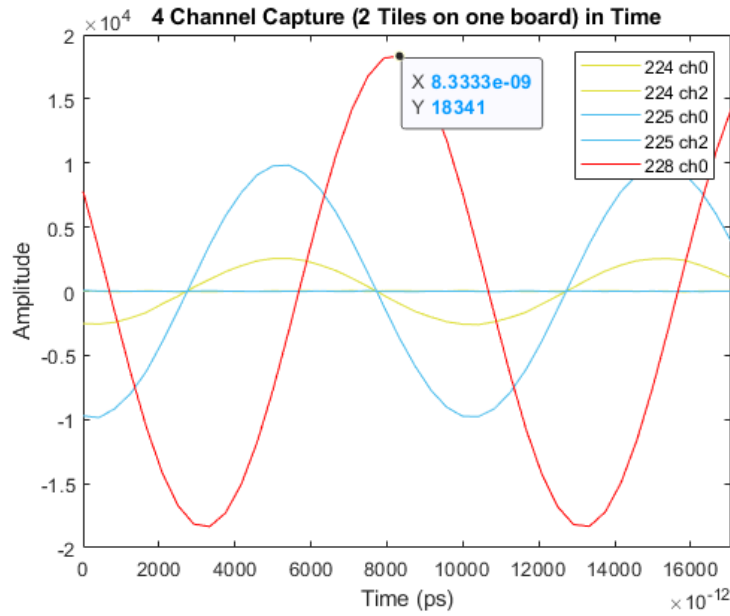
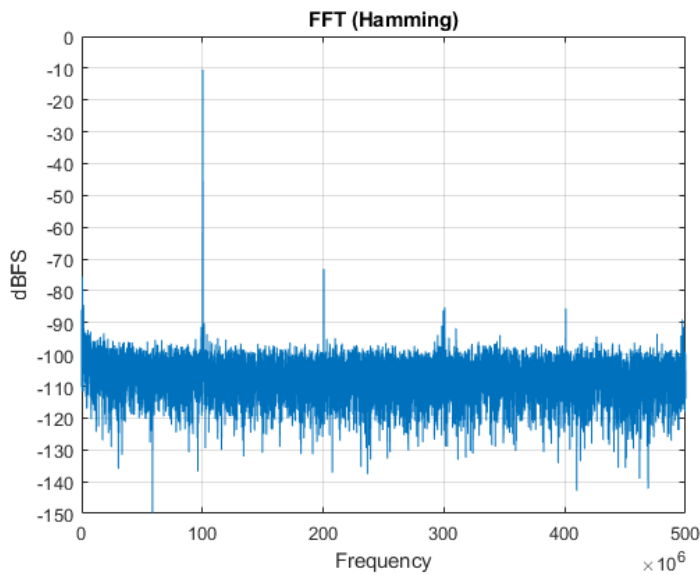


Figure 4.2.: RF DC Evaluation Tool GUI [Xil20a]



**Figure 4.3.:** Placeholder



**Figure 4.4.:** Placeholder

## 5. Conclusions and Outlook

### 5.1. Measurements with the developed front-end card

Card is in production. Measurements will be done, but not in the scope of the thesis.

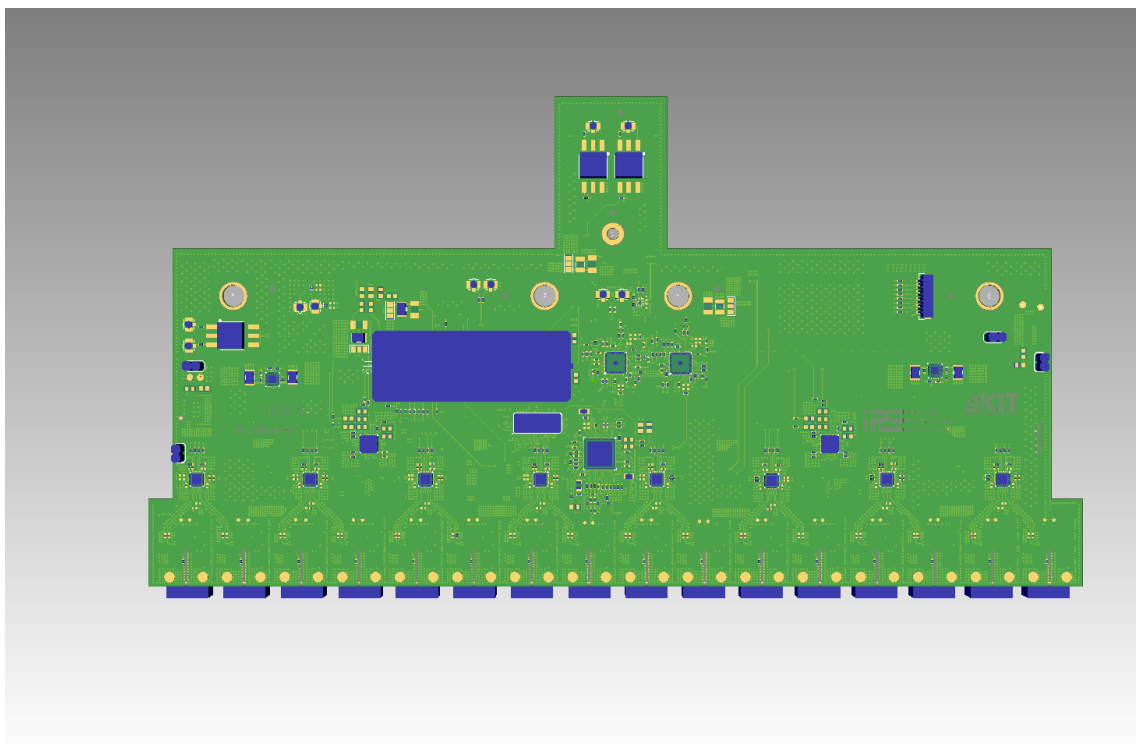


**Figure 5.1.:** wow



## Acknowledgments



# Appendix

## A. QuickStart Guide for Evaluation of ZCU216 Board

### B. 3D model of front-end card

### C. Code

```
'timescale 1ns / 1ps

module SDI_Delay_NB6L295(
    // data for respective delay chips
    input [10:0]           In_1, In_2, In_3, In_4, In_5, In_6, In_7, In_8,
    input                 Clk,
    input                 Reset,
    output reg [7:0]       EN,
    // enable signal for delay chips, active LOW
    output reg             SDIN,
    // configuration data
    output reg             SLOAD,
    // signals delay chip to load previously sent data
    output                SCLK
    // clock for serial communication with delay chips
);
);

reg                      start_clk;
assign SCLK = start_clk & (!Clk);

reg [21:0]           In_1_reg, In_2_reg, In_3_reg, In_4_reg, In_5_reg, In_6_reg, In_7_reg, In_8_reg;
// registers to intermediately store the inputs

reg [7:0]           select;
// register used by Priority Encoder to detect which input changed

parameter            DATA_SHIFT_WIDTH = 11;
// number of bits to be shifted during transmission, 1 Data word = 11 bits
reg [4:0]           clk_cnt;

// reg [DATA_SHIFT_WIDTH-1:0] Data_reg;
// register for storing data for state machine

reg                  start;
// signal for state machine to start sending data
reg                  dataSent;
// flags if transmission for one delay chip is finished

parameter            dly = 1;
// delay control

reg                  delayReady;

always @ (posedge Clk)
begin
    if (select == 'd0)      delayReady <= #dly 'b1;
    else                     delayReady <= #dly 'b0;
end

// Priority Encoder
// Check if any input has changed, select which data should be sent accordingly
always @ (posedge Clk)
begin
    if (Reset)
        begin
            In_1_reg      <= #dly 'd0;
            In_2_reg      <= #dly 'd0;
            In_3_reg      <= #dly 'd0;
            In_4_reg      <= #dly 'd0;
            In_5_reg      <= #dly 'd0;
            In_6_reg      <= #dly 'd0;
            In_7_reg      <= #dly 'd0;
            In_8_reg      <= #dly 'd0;
            Data_reg      <= #dly 'd0;

            select         <= #dly 'd0;
            start          <= #dly 1'b0;;
        end
end
```

```

else
begin
  if (~start & delayReady)
begin
  select [7]    <= #dly In_1_reg != In_1;
  select [6]    <= #dly In_2_reg != In_2;
  select [5]    <= #dly In_3_reg != In_3;
  select [4]    <= #dly In_4_reg != In_4;
  select [3]    <= #dly In_5_reg != In_5;
  select [2]    <= #dly In_6_reg != In_6;
  select [1]    <= #dly In_7_reg != In_7;
  select [0]    <= #dly In_8_reg != In_8;
end
else
begin
  if (clk_cnt == 4'd12 & ~start_clk) // = end of sequence
    start      <= #dly 1'b0;
  else
    start      <= #dly 1'b1;
end

casex (select)
  8'b1???????
begin
  if (~dataSent)
begin
  In_1_reg      <= #dly In_1;
  Data_reg      <= #dly In_1;
  EN            <= #dly 8'b01111111;
  start          <= #dly 1'b1;
end
else
begin
  start          <= #dly 1'b0;
  select [7]     <= #dly 1'b0;
end
end
  8'b01??????
begin
  if (~dataSent)
begin
  In_2_reg      <= #dly In_2;
  Data_reg      <= #dly In_2;
  EN            <= #dly 8'b10111111;
  start          <= #dly 1'b1;
end
else
begin
  select [6]     <= #dly 1'b0;
  start          <= #dly 1'b0;
end
end
  8'b001?????
begin
  if (~dataSent)
begin
  In_3_reg      <= #dly In_3;
  Data_reg      <= #dly In_3;
  EN            <= #dly 8'b11011111;
  start          <= #dly 1'b1;
end
else
begin
  select [5]     <= #dly 1'b0;
  start          <= #dly 1'b0;
end
end
  8'b0001?????
begin
  if (~dataSent)
begin
  In_4_reg      <= #dly In_4;
  Data_reg      <= #dly In_4;
  EN            <= #dly 8'b11101111;
  start          <= #dly 1'b1;
end
else
begin
  select [4]     <= #dly 1'b0;
  start          <= #dly 1'b0;
end
end
  8'b00001???
begin
  if (~dataSent)
begin
  In_5_reg      <= #dly In_5;
  Data_reg      <= #dly In_5;
  EN            <= #dly 8'b11110111;
  start          <= #dly 1'b1;
end
else
begin
  select [3]     <= #dly 1'b0;
  start          <= #dly 1'b0;
end
end
  8'b000001??:
```

```

begin
  if (~dataSent)
    begin
      In_6_reg           <= #dly In_6;
      Data_reg           <= #dly In_6;
      EN                 <= #dly 8'b11111011;
      start              <= #dly 1'b1;
    end
  else
    begin
      select [2]         <= #dly 1'b0;
      start              <= #dly 1'b0;
    end
  end
  8'b00000001?:
  begin
    if (~dataSent)
      begin
        In_7_reg           <= #dly In_7;
        Data_reg           <= #dly In_7;
        EN                 <= #dly 8'b11111101;
        start              <= #dly 1'b1;
      end
    else
      begin
        select [1]         <= #dly 1'b0;
        start              <= #dly 1'b0;
      end
  end
  8'b000000001:
  begin
    if (~dataSent)
      begin
        In_8_reg           <= #dly In_8;
        Data_reg           <= #dly In_8;
        EN                 <= #dly 8'b11111110;
        start              <= #dly 1'b1;
      end
    else
      begin
        select [0]         <= #dly 1'b0;
        start              <= #dly 1'b0;
      end
  end
  default:
    begin
      EN                 <= #dly 8'b11111111;
      start              <= #dly 1'b0;
    end
  endcase
end
// State Machine for Sending Configuration Data to Delay Chip NB6L295
/*
 *          State          Description
 */
RESET          Resetting all parameters and registers -> if (reset): stay; else: to IDLE
IDLE           Waiting for start signal from priority encoder -> if (start): to LOAD_P0; else: stay
LOAD_P0        Load first half of Delay_X - which corresponds to data for Delay PD0 on delay chip
LOAD_P1        Load second half of Delay_X - which corresponds to data for Delay PD1 on delay chip
SHIFT          Shift bits for sending serial bitstream to SDIN, assert SLOAD -> to END
END            End transmission, deassert SLOAD, inform priority encoder about end of transmission
*/
parameter RESET      = 3'd0;
parameter IDLE       = 3'd1;
parameter LOAD        = 3'd2;
parameter SHIFT       = 3'd3;
parameter END         = 3'd4;
reg [2:0] STATE;     tmp;
reg [DATA_SHIFT_WIDTH-1:0]

always @ (posedge Clk)
begin
  if (Reset)
    begin
      STATE      <= #dly RESET;
      tmp        <= #dly 'd0;
      dataSent   <= #dly 1'b0;
      start_clk  <= #dly 1'b0;
      SLOAD      <= #dly 1'b0;
      clk_cnt    <= #dly 1'b0;
    end
  else
    begin
      case (STATE)
        RESET:
          begin
            if (Reset)
              STATE    <= #dly RESET;
            else
              STATE    <= #dly IDLE;
          end // RESET
        IDLE:
          begin
            SDIN     <= #dly 1'b0;
            clk_cnt  <= #dly 5'd0;
          end
      endcase
    end
  end
end

```

```

dataSent      <= #dly 1'b0;
SLOAD        <= #dly 1'b0;

if (start & ~dataSent)
    STATE    <= #dly LOAD;
else
    STATE    <= #dly IDLE;
end // IDLE
LOAD:
begin
    tmp          <= #dly Data_reg;
    STATE        <= #dly SHIFT;
end // LOAD_W1
SHIFT:
begin
    if (clk_cnt < 4'd12) // number of bits to be shifted //
        begin
            start_clk      <= #dly 1'b1;
            clk_cnt        <= #dly clk_cnt +1;
            tmp           <= #dly {tmp[DATA_SHIFT_WIDTH-2:0], 1'b0};
            SDIN          <= #dly tmp[DATA_SHIFT_WIDTH-1];
        end
    else
        begin
            SLOAD        <= #dly 1'b1;
            clk_cnt      <= #dly clk_cnt;
            start_clk    <= #dly 1'b0;
            STATE        <= #dly END;
            SDIN          <= #dly 1'b0;
        end
    end // SHIFT
END:
begin
    SLOAD        <= #dly 1'b0;
    start_clk    <= #dly 1'b0;
    dataSent     <= #dly 1'b1;
    clk_cnt      <= #dly clk_cnt;
    SDIN          <= #dly 1'b0;
    STATE        <= #dly IDLE;
end // END
default:
    STATE    <= #dly RESET;
endcase
end
endmodule

```

# Bibliography

- [BBB<sup>+</sup>19] Bielawski, Serge, Edmund Blomley, Miriam Brosi, Erik Bründermann, Eva Burkard, Clément Evain, Stefan Funkner, Nicole Hiller, Michael Nasse, Guadrun Niehues und et al.: *From self-organization in relativistic electron bunches to coherent synchrotron light: observation using a photonic time-stretch digitizer.* Scientific Reports, 9(1), July 2019. <http://dx.doi.org/10.1038/s41598-019-45024-2>.
- [Bro20] Brosi, Miriam: *In-Depth Analysis of the Micro-Bunching Characteristics in Single and Multi-Bunch Operation at KARA.* Dissertation, Karlsruher Institut für Technologie (KIT), 2020. 54.01.01; LK 01.
- [BSMM99] Bronstein, Semendjajew, Musiol und Mühlig: *Taschenbuch der Mathematik.* Verlag Harri Deutsch, 1999.
- [CAB<sup>+</sup>17] Caselle, M., L.E. Ardila Perez, M. Balzer, A. Kopmann, L. Rota, M. Weber, M. Brosi, J. Steinmann, E. Bründermann und A. S. Müller: *KAPTURE-2. A picosecond sampling system for individual THz pulses with high repetition rate.* Journal of Instrumentation, 12, 2017.
- [Gmb] GmbH, LD DIDACTIC: *Demonstrating the Pockels effect in a conoscopic beam path.* [https://www.ld-didactic.de/literatur/hb/e/p5/p5451\\_e.pdf](https://www.ld-didactic.de/literatur/hb/e/p5/p5451_e.pdf).
- [Kes05] Kester, Walt: *The Data Conversion Handbook.* Newnes, 2005.
- [LV02] Lundberg, Kent H. und Vin Vq: *Analog-to-Digital Converter Testing,* 2002.
- [MR15] Manganaro, Gabriele und Dave Robertson: *Interleaving ADCs: Unraveling the Mysteries.* Analog Dialogue, 2015.
- [Pue15] Puente León, Fernando: *Messtechnik - Systemtheorie für Ingenieure und Informatiker.* Vieweg Verlag, 10. aufl. Auflage, 2015, ISBN 978-3-662-44820-5.
- [Rot18] Rota, Lorenzo: *KALYPSO, a novel detector system for high-repetition rate and real-time beam diagnostics.* Dissertation, Karlsruher Institut für Technologie (KIT), 2018. 54.02.02; LK 01.
- [Rou14] Roussel, Eleonore: *Spatio-temporal dynamics of relativistic electron bunches during the microbunching instability: study of the Synchrotron SOLEIL and UVSOR storage rings.* Dissertation, September 2014.
- [SELP<sup>+</sup>16] Szwaj, C., C. Evain, M. Le Parquier, P. Roy, L. Manceron, J. B. Brubach, M. A. Tordeux und S. Bielawski: *High sensitivity photonic time-stretch electro-optic sampling of terahertz pulses.* Review of Scientific Instruments, 87(10), 2016.
- [Wad91] Wadell, Brian C.: *Transmission Line Design Handbook.* Artech House, 1991.

- [Xil20a] Xilinx: *UG1433 - Zynq UltraScale+ RFSoCZCU208 and ZCU216 RFData Converter Evaluation Tool User Guide.* [https://www.xilinx.com/support/documentation/boards\\_and\\_kits/zcu216/ug1433-zcu216-rfsoc-eval-tool.pdf](https://www.xilinx.com/support/documentation/boards_and_kits/zcu216/ug1433-zcu216-rfsoc-eval-tool.pdf), June 2020.
- [Xil20b] Xilinx: *UG1437 - CLK104 RF Clock Add-onCard User Guide.* [https://www.xilinx.com/support/documentation/boards\\_and\\_kits/zcu216/ug1437-clk104.pdf](https://www.xilinx.com/support/documentation/boards_and_kits/zcu216/ug1437-clk104.pdf), March 2020.